



Pressure-induced reversible transformation in single-wall carbon nanotube bundles studied by Raman spectroscopy

Pallavi V. Teredesai^a, A.K. Sood^{a,b,*}, D.V.S. Muthu^a, R. Sen^b, A. Govindaraj^b,
C.N.R. Rao^b

^a Department of Physics, Indian Institute of Science, Bangalore 560 012, India

^b Jawaharlal Nehru Center for Advanced Scientific Research, Jakkur Campus, Jakkur P.O., Bangalore 560 064, India

Received 16 June 1999

Abstract

We report our high-pressure Raman studies on single-wall carbon nanotube bundles carried out up to 25.9 GPa. The intensity of the radial modes decreases more drastically as compared to that of the tangential modes. The former could be followed up in pressure runs to 3 GPa. The most intriguing observation is the anomalous pressure behaviour of the 1594 cm^{-1} tangential mode between 10 and 16 GPa. This feature, as well as the pressure dependence of intensity, peak position and linewidth, are reversible on decompression. The anomalous pressure dependence is argued to be associated with faceting of the tubes in the bundle, showing their remarkable resilience. © 2000 Elsevier Science B.V. All rights reserved.

1. Introduction

Novel properties such as unusual mechanical strength and one-dimensional electronic transport in single-wall carbon nanotubes (SWNT) have been studied actively in recent years, both experimentally and theoretically [1]. Experimental studies have been made possible due to the synthesis of bundles of aligned SWNT with narrow-size distribution in large quantities by laser pulse vaporization [2], followed by the electric arc method [3]. A SWNT made from rolling a graphene sheet up into a cylinder with caps made up of C_{60} hemispheres can be specified in

terms of chiral vector $na_1 + ma_2$ and chiral angle θ given by $\tan^{-1}(\sqrt{3}m/(m+2n))$. Here a_1 and a_2 are primitive lattice vectors of a 2D hexagonal honeycomb lattice and m, n are integers. The tube has chiral symmetry for $n \neq m \neq 0$ and achiral tubes with $m = 0$ and $n = m$ are called zigzag and arm-chair tubes, respectively. The diameter of the SWNT is related to the (n, m) values by $d = a[3(n^2 + m^2 + mn)]^{1/2}/\pi$, where a is the nearest C–C distance ($= 1.42 \text{ \AA}$). Recent scanning tunneling spectroscopy experiments [4,5] have verified the theoretical predictions that the electronic properties of SWNT are given by one-dimensional density of states. These isolated tubes can be semiconducting or metallic, depending on their diameter and the chiral angle [1]. Isolated tubes are metallic when $(n - m)/3$ is an integer. Intertube interaction between the tubes in a

* Corresponding author. Fax: +91-80-3602602; e-mail: asood@physics.iisc.ernet.in

bundle enhances density of states near the Fermi level [6]. In addition, a pseudogap of ~ 0.1 – 0.2 eV is introduced near E_F in the density of states [7] due to breaking of the D_{10h} tube symmetry by the triangular lattice of the bundle. The pseudogap is reduced due to orientational and other types of disorder [6].

Raman spectroscopy, in particular resonant Raman, has played a key role in understanding the vibrational and electronic properties of fullerenes and SWNT, especially the one-dimensional nature of the electronic properties of the latter [8]. Pristine graphite with D_{6h}^4 symmetry shows nine vibrational optic modes given in terms of irreducible representation by $2E_{2g}(R) + 2B_{1g} + A_{2u}(IR) + E_u(IR)$ where R and IR denote Raman-active and infrared-active modes, respectively. The E_{2g} modes are at $\omega \sim 1579$ cm^{-1} associated with out-of-phase intralayer displacement of carbon atoms and $\omega \sim 44$ cm^{-1} associated with in-phase interlayer displacement of carbon atoms resulting in rigid shearing motion between graphite layers. The Raman spectrum of a SWNT can be broadly divided into two parts: a low-frequency radial mode around 180 cm^{-1} and a high-frequency tangential mode around 1590 cm^{-1} . The radial band is sensitive to diameter, irrespective of the chirality of the tube. It has been shown that the position and the Raman lineshape of the radial mode depends significantly on the exciting laser energy as a result of a diameter-selective resonance Raman scattering process [9].

Hexagonal graphite has lowest internal energy and hence is the equilibrium structure of carbon at ambient conditions. Pressure-induced phase transitions under static and dynamic loading between the many allotropes of carbon like cubic diamond, hexagonal diamond, graphite, fullerenes C_{60} and C_{70} and their polymeric and amorphous forms are of great scientific interest as well as have practical importance. Earlier we have used Raman spectroscopy to explore the pressure and temperature-induced orientational phase transitions in solid C_{60} and solid C_{70} , [10–13], pressure-induced amorphisation of solid C_{70} [14] and pressure–temperature-induced polymeric phases [15,16]. The main focus of this Letter is to discuss our results on pressure effects on SWNT bundles probed using Raman spectroscopy up to a maximum pressure of 25.9 GPa in a diamond anvil cell. After the completion of our work, we

came across the work of Venkateswaran et al. [17] on SWNT bundles carried up to ~ 5 GPa. We make comparisons of our data with the numerical simulations and data reported by Venkateswaran et al.

2. Experimental details

SWNT bundles were prepared by the arc discharge method similar to that of Jorret et al. [3]. A graphite rod (length, 6 cm; diameter, 6 mm) with a hole (diameter, 4 mm) drilled in it was filled with a mixture of graphite powder, Y_2O_3 (1 at % Y) powder and Ni (4.2 at % Ni) powder and a composite rod made in this way was treated with a H_2 atmosphere at 1000 °C. This composite graphite rod was used as an anode in the arc chamber along with a simple graphite rod as cathode. Arcing was carried out using a dc power source (20 V, 70 Amp) under a helium atmosphere of 660 Torr. Copious quantities of web-like material deposited inside the arc chamber were removed, washed with CS_2 and heated in air at 300 °C for 24 h, to burn out amorphous carbon deposits. This was stirred with concentrated HCl acid for 24 h at 50 °C to remove metal particles present along with the SWNT. After decantation and washing with distilled water, the sample was dried and suspended in ethanol using an ultrasound sonicator. To separate the SWNT from small graphitic nanoparticles, this ethanol suspension was filtered using a Millipore microfilter with pore size of 0.3 μm . The resulting pure SWNT collected on the filter paper were dried at 100 °C and characterised by transmission electron microscopy [18]. The average diameter of the tubes in the bundles obtained is 1.4 nm.

High-pressure Raman experiments were carried out at room temperature up to 25.9 GPa in a gasketed Mao–Bell-type diamond anvil cell (DAC) with a pressure-transmitting medium of methanol/ethanol/water in 16:3:1 proportion. Pressure was measured in situ by the well-known ruby fluorescence technique [19]. A laser line from an argon ion laser at 5145 Å at a power of ~ 25 mW (on the face of the diamond) was used to excite the Raman spectra. The scattered light from the sample was collected in the back-scattering geometry, and analysed using a computer-controlled double-grating

monochromator (Spex Ramalog 5) equipped with a Peltier cooled photomultiplier tube and the photon counting system. The spectral resolution was 5 cm^{-1} and each data point was averaged over a period of 5 s to improve the signal-to-noise ratio.

3. Results and discussion

Figs. 1 and 2 show typical Raman spectra of the SWNT bundle recorded at different pressures in the radial and tangential mode regions, respectively. The spectra at 0.1 GPa are similar to those reported

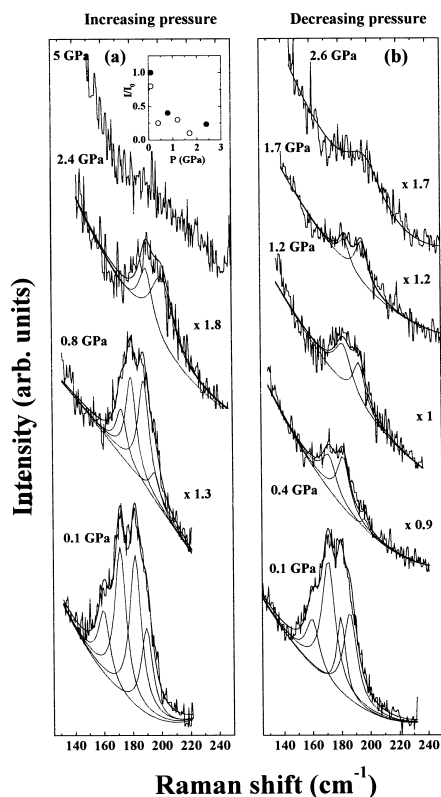


Fig. 1. Raman spectra of a SWNT bundle in radial mode region at different pressures in (a) increasing and (b) decreasing pressure runs. The individual fitted Lorentzian peaks are shown with dotted lines. The inset in (a) shows the intensity of 172 cm^{-1} mode normalised with its value at 0.1 GPa as a function of pressure, in increasing (filled circles) and decreasing (open circles) pressure runs.

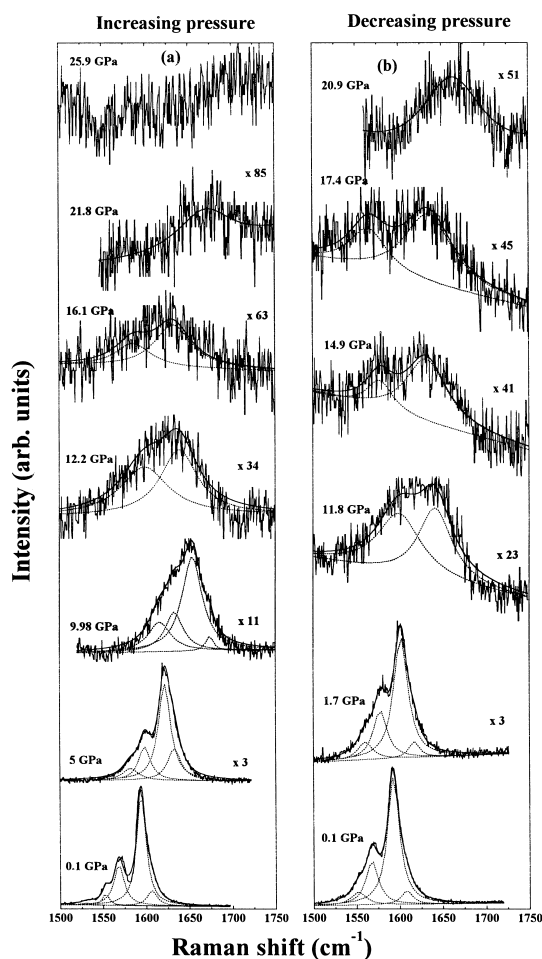


Fig. 2. Raman spectra of SWNT bundle in tangential mode region at different pressures in (a) increasing and (b) decreasing pressure runs. The individual Lorentzian fits are shown with dotted lines.

earlier at atmospheric pressure [8]. The two dominant radial bands in the spectrum recorded at 0.1 GPa occur at 172 and 182 cm^{-1} (lowest curve in Fig. 1a). For an isolated SWNT, the calculated frequencies of the radial mode have been empirically fitted to $\omega_R(\text{cm}^{-1}) = 223.75/d(\text{nm})$, irrespective of the nature of the tube [20]. This gives $\omega_R = 164.8 \text{ cm}^{-1}$ for (10,10) and 183.1 cm^{-1} for the (9,9) tube. These frequencies are, however, different from the recent simulation results obtained using generalised tight binding molecular dynamics. The inclusion of Van der Waals interaction between the (9,9) tubes shifts

the radial mode frequency from 171.8 cm^{-1} (for an isolated tube) to 186.2 cm^{-1} . It has been suggested [17] that this blue shift of 14.4 cm^{-1} due to intertube interaction is independent of the tube diameter. Accordingly, we suggest an empirical relation for tube diameter dependence of the radial mode frequency in a SWNT bundle: $\omega_R(\text{cm}^{-1}) = 14.4 + 209.9/d(\text{nm})$ which retains the $1/d$ dependence of ω_R and reproduces $\omega_R = 186.2 \text{ cm}^{-1}$ for the (9,9) tube [17]. It has been observed that (10,10) tubes are most abundantly produced [2,21] which has been rationalised based on the diameter selection due to the competition between the strain energy of the curvature of the graphite sheet and dangling-bond energy of the open edge. The arm-chair configuration is energetically favoured for which the C–C bonds are perpendicular to the axis of the tube. Keeping this in mind, the radial mode at 172 cm^{-1} in Fig. 1a can be associated with (10,10) tubes in SWNT bundles. The tangential modes in Fig. 2 are assigned in terms of irreducible representations of D_{nh} (D_{nd}) for even n (odd n), with 1531 cm^{-1} as E_{1g} , 1553 cm^{-1} and 1568 cm^{-1} as E_{2g} , 1594 cm^{-1} with unresolved doublet $A_{1g} + E_{1g}$ and 1606 cm^{-1} with E_{2g} symmetry [8,22]. Subsequently, in this Letter, these peak positions will be used to refer to the tangential modes.

As can be seen in Fig. 1a, the intensities of the radial modes fall rapidly with increasing pressure, so much so that the modes were not discernible in the recorded spectra beyond 2.6 GPa. The inset shows the intensity of the 172 cm^{-1} mode normalised with its value at 0.1 GPa as a function of pressure (filled circles for increasing pressure and open circles for decreasing pressure). Fig. 1b shows the Raman spectra after cycling the sample from the maximum pressure of 25.9 GPa. It can be seen that the Raman features are reversible. As for radial modes, the intensities of the tangential modes also decrease with pressure. The spectra could be resolved into 4 bands up to 10 GPa, beyond which they could be fitted with 2 Lorentzian functions up to ~ 16 GPa. At higher pressures, the observed bands were very weak and broad and could be fitted with only 1 Lorentzian.

Fig. 3 shows the pressure dependence of the 172 cm^{-1} radial mode in the increasing (filled squares) and decreasing (open squares) pressure runs, along with the calculated curves for three models [17] (to be discussed later). The tangential mode frequencies

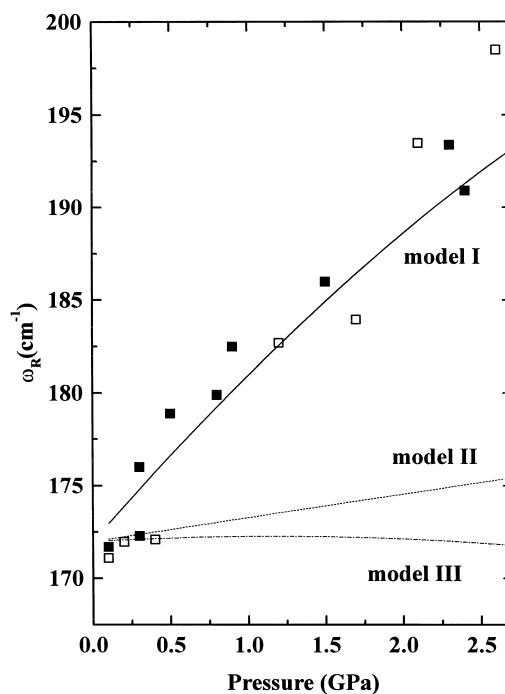


Fig. 3. Pressure variation of the radial mode frequency. The solid squares (open squares) indicate the increasing (decreasing) pressure run. The theoretical curves for models I, II and III are shown [17].

are plotted as a function of pressure in Fig. 4a–c. Most interestingly, it is seen that the modes at 1568 cm^{-1} (Fig. 4b) and 1594 cm^{-1} (most intense mode, Fig. 4c) show softening between ~ 10 – 16 GPa. Beyond 16 GPa, the broad band peak position increases with pressure, as shown in Fig. 4b,c. Remarkably, when the pressure is reduced from the highest pressure of 25.9 GPa, the peak positions (shown by open symbols in Fig. 4) follow the same trend as in the increasing pressure run. The intensity of the 1594 cm^{-1} mode normalised with respect to its value at 0.1 GPa (I/I_0) and its full width at half maximum (FWHM) are shown as a function of pressure in Fig. 5a,b in increasing (solid circles) and decreasing pressure runs (open circles), demonstrating that the features of the tangential mode are also reversible on release of pressure. The values of the slope $d\omega/dP$ obtained by fitting $\omega(P) = \omega(0) + aP$ to the tangential modes and a second-order polynomial to the radial mode have been used to calculate a

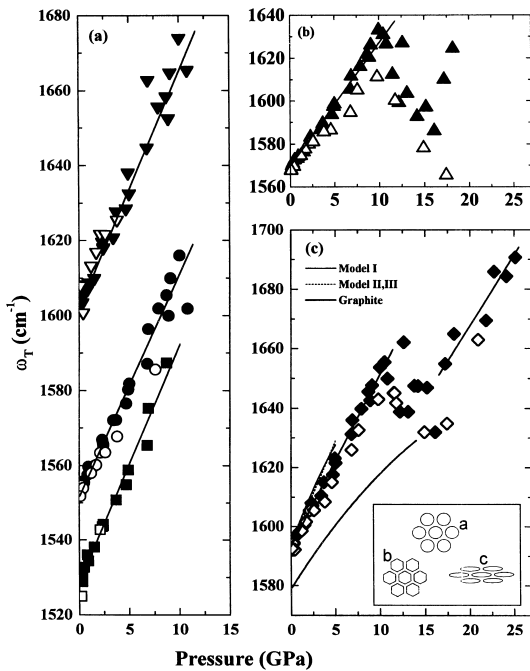


Fig. 4. (a) Pressure variation of 1531, 1553 and 1606 cm^{-1} mode frequencies. (b) Pressure variation of 1568 cm^{-1} mode frequency. (c) Pressure variation of 1594 cm^{-1} mode frequency. Data for the increasing pressure (filled points) and decreasing pressure (open points) are fitted to first order polynomial $\omega(P) = \omega(0) + aP$. The theoretical curves for the three models are plotted up to 5 GPa [17]. Pressure dependence of the 1579 cm^{-1} mode of graphite is also shown [24]. The inset shows the faceting in SWNT bundle leading to the conversion of (a) circular cross-section to (b) hexagonal and (c) elliptical cross-sections.

mode Grüneisen parameter $\gamma_i = Bd \ln \omega / dP$ where B is the bulk modulus of the SWNT bundle. The value of B has been taken to be 13 GPa from experimental measurements of pressure dependence of density, which is about 4 times lower than the calculated value [23]. The experimental value of B for graphite is 33.8 GPa [24], almost 2.5 times that of SWNT bundle. Table 1 shows that the slope $d\omega/dP$ for the tangential mode is similar to 1579 cm^{-1} mode of graphite, but the value of the Grüneisen parameter is half that of graphite, simply due to differences in the values of the bulk modulus B . The γ value for the radial mode at 172 cm^{-1} is 0.73. This large difference (\sim factor of 15) between the values of γ for tangential and radial modes is

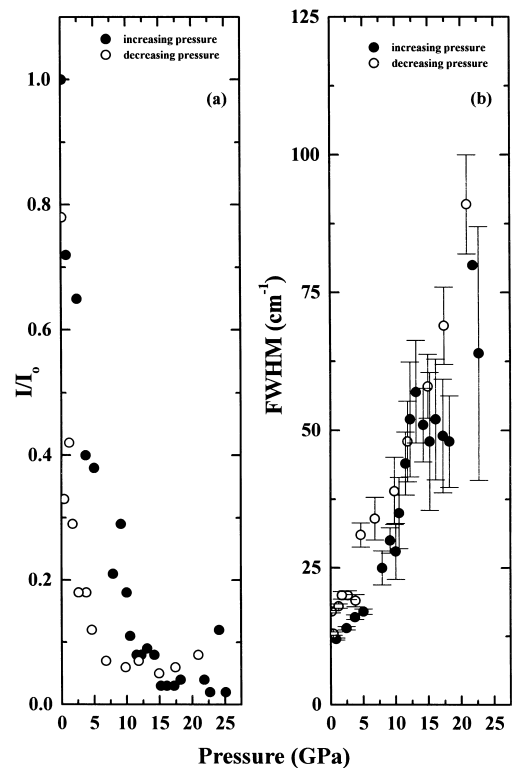


Fig. 5. (a) The intensity of 1594 cm^{-1} mode normalised with respect to its value at 0.1 GPa as a function of pressure. (b) The FWHM as a function of pressure. Error bars are shown for each data point indicating large errors for higher pressure values.

similar to the case of graphite (for the two E_{2g} modes at 1579 and 44 cm^{-1}) and other layered as

Table 1

Grüneisen parameters for the five tangential and one radial modes in SWNT bundle. The two values of $d\omega/dP$ and γ shown for mode 4 correspond to $P < 14$ GPa and $P > 14$ GPa, respectively. For comparison, the values for the modes in graphite are also given from Ref. [24].

Mode	$\omega(0)$ (cm^{-1})	$d\omega/dP$ ($\text{cm}^{-1}/\text{GPa}$)	γ
Mode 1	1529	6.3	0.054
Mode 2	1553	5.7	0.048
Mode 3	1569	5.7	0.047
Mode 4	1595	5.3	0.043
		4.2	0.034
Mode 5	1603	6.5	0.053
Radial mode	172	9.6	0.73
Graphite	1579	4.7	0.1
	44	4.8	3.7

well as molecular crystals [25]. For the latter, the values are $\gamma \sim 1$ for external vibrations and $\gamma \ll 1$ for intramolecular internal vibrational modes.

We now come to discuss the pressure dependence of intensities, linewidths and mode frequencies. The pressure-induced changes in energy difference between singularities in the valence and conduction bands in the 1D density of electronic states will reduce the resonance enhancement in the Raman cross-section. This can be the reason for the decrease in the intensities of radial and tangential modes under pressure. The enhanced intertube interactions at higher pressures resulting in increased density of electronic states near the Fermi level can also contribute to reduced Raman intensities. The latter will also result in increased phonon linewidths. Venkateswaran et al. [17] have used generalised tight binding molecular dynamics simulations to calculate the pressure dependence of the radial and tangential modes up to 5 GPa. They have considered three situations for pressure transmittance to the SWNT bundle. Model I takes uniform external radial compression of the entire triangular lattice which corresponds to the situation that the pressure-transmitting medium is not present in the interstitial channels in the tube lattice. This is not the case in models II and III where all the individual nanotubes in a triangular lattice feel the pressure medium. However, in model II, intertube interactions are ignored and therefore the compression is symmetric for all tubes whereas these interactions are included in model III. Like Ref. [17], the pressure dependence of the radial mode is consistent with only model I as shown in Fig. 3. This is rather surprising because the assumption of non-penetration of the pressure-transmitting fluid inside the bundle is inconsistent with the small blue shift of the radial mode frequency ($\sim 2\text{--}4\text{ cm}^{-1}$) when SWNT bundles are soaked in alcohol mixture [26]. For tangential modes, the prediction of models I, II and III are similar as shown in Fig. 4c. The calculations, done only up to 5 GPa, had included intertube Van der Waals interactions in the usual Lennard-Jones form. At higher pressures, electron hopping between the tubes has to be taken into account and hence the results of Ref. [17] cannot be extrapolated to higher pressures.

At this stage, we do not understand the origin of the anomalous pressure dependence of the 1568 and

1594 cm^{-1} modes between 10 and 16 GPa. In order to get some clues, we note that valence-force model calculations [27] of the structural properties of a carbon nanotube crystal reveal that for tube diameters above 25 Å, the tubes flatten against each other forming a honeycomb structure. It has been suggested [23] that, under pressure, smaller diameter tubes can also facet and the tube cross-section can change from circular to hexagonal or elliptical, as shown in the inset of Fig. 4c. This will considerably affect the Raman intensities of the modes, more so for the radial one, as seen in our experiments. The faceting will result in considerable overlap of the surfaces of the neighbouring tubes, similar to the stacking of two AB planes in graphite. The tangential mode frequencies in the SWNT bundle then will be close to the E_{2g} in-plane vibration of graphite at 1579 cm^{-1} . The pressure dependence of the E_{2g} 1579 cm^{-1} mode of graphite [24] measured to 14 GPa is shown by the thick solid line in Fig. 4c. It is indeed seen that the frequency of the 1594 cm^{-1} mode of the SWNT bundle starts approaching that of graphite at ~ 10 GPa and this process is completed at ~ 16 GPa. Beyond 16 GPa, the pressure derivative $d\omega/dP$ is similar to that of graphite [24] to the highest pressure reached in our experiments. Since graphite is known to transform to amorphous carbon at 23 GPa [28] which reverts to the crystalline form on release of pressure [29], we believe that the SWNT bundle does not transform to bulk graphite under hydrostatic pressure, as is evident from the reversibility of the Raman spectra of the pressure cycled SWNT bundle. We conclude that the faceting of the tubes in the bundle is the reason behind the anomalous pressure dependence of the tangential mode frequency. Our experiments show that the pressure effects are reversible on release of as high a pressure as 25.9 GPa, implying that the nanotubes are highly resilient and regain their shape when decompressed. This is similar to the high-resolution electron microscope observations and atomistic simulations of the bending of SWNT under mechanical stress which reveal remarkable flexibility of the hexagonal network that resists bond breaking and bond stretching up to very high strain values [30]. It is desirable to extend the calculations of pressure effects to very high pressures, as in the present studies, and to carry out high-pressure X-ray diffrac-

tion experiments to look for faceting and other pressure effects.

Acknowledgements

A.K.S. thanks the Department of Science and Technology, India, for financial assistance. P.V.T. thanks the Council for Scientific and Industrial Research, India, for the award of a fellowship.

References

- [1] M.S. Dresselhaus, G.F. Dresselhaus, P.C. Eklund, *Science of Fullerenes and Carbon Nanotubes*, Academic Press, New York, 1996, Chap. 19.
- [2] A. Thess, R. Lee, P. Nikolaev, H. Dai, P. Petit, J. Robert, C. Xu, Y.H. Lee, S.G. Kim, A.G. Rinzler, D.T. Colbert, C.E. Scuseria, D. Tomanek, J.E. Fischer, R.E. Smalley, *Science* 273 (1996) 483.
- [3] C. Journet, W.K. Maser, P. Bernier, A. Loiseau, M. Lamy de la Chapelle, S. Lefrant, P. Denierd, R. Lee, J.E. Fischer, *Nature (London)* 388 (1997) 756.
- [4] J.W.C. Wildoer, L.C. Venema, A.G. Rinzler, R.E. Smalley, C. Dekker, *Nature (London)* 391 (1998) 59.
- [5] T.W. Odom, J.L. Huang, P. Kim, C.M. Lieber, *Nature (London)* 391 (1998) 62.
- [6] Y.K. Kwon, D. Tomanek, Y.H. Lee, S. Saito, *J. Mater. Res.* 13 (1998) 2363.
- [7] P. Delaney, H.J. Choi, J. Ihm, S.G. Louie, M.L. Cohen, *Nature (London)* 391 (1998) 466.
- [8] A.M. Rao, E. Richter, S. Bandow, P.C. Eklund, K.A. Williams, S. Fang, K.R. Subbaswamy, M. Menon, A. Thess, R.E. Smalley, G. Dresselhaus, M.S. Dresselhaus, *Science* 275 (1997) 187.
- [9] M.A. Pimenta, A. Marucci, S.D.M. Brown, M.J. Matthews, A.M. Rao, P.C. Eklund, R.E. Smalley, G. Dresselhaus, M.S. Dresselhaus, *J. Mater. Res.* 13 (1998) 2396.
- [10] N. Chandrabhas, M.N. Shashikala, D.V.S. Muthu, A.K. Sood, C.N.R. Rao, *Chem. Phys. Lett.* 197 (1992) 319.
- [11] N. Chandrabhas, K. Jayram, D.V.S. Muthu, A.K. Sood, R. Sheshadri, C.N.R. Rao, *Phys. Rev. B (Rapid Commun.)* 47 (1993) 10963.
- [12] S.K. Ramsesha, A.K. Singh, R. Sheshadri, A.K. Sood, C.N.R. Rao, *Chem. Phys. Lett.* 220 (1994) 203.
- [13] A.K. Sood, N. Chandrabhas, D.V.S. Muthu, C.S. Sunder, A. Bharati, Y. Hariharan, C.N.R. Rao, *Phil. Mag. B* 70 (1994) 347.
- [14] N. Chandrabhas, A.K. Sood, D.V.S. Muthu, C.S. Sunder, A. Bharathi, Y. Hariharan, C.N.R. Rao, *Phys. Rev. Lett.* 73 (1994) 3411.
- [15] C.S. Sunder, P.Ch. Sahu, V. S Sastry, G.V.N. Rao, V. Sridharan, M. Premila, A. Bharathi, Y. Hariharan, T.S. Radhakrishnan, D.V.S. Muthu, A.K. Sood, *Phys. Rev. B* 53 (1996) 8180.
- [16] M. Premila, C.S. Sunder, P.Ch. Sahu, A. Bharathi, Y. Hariharan, D.V.S. Muthu, A.K. Sood, *Solid State Commun.* 104 (1997) 237.
- [17] U.D. Venkateswaran, A.M. Rao, E. Richter, M. Menon, A. Richter, R.E. Smalley, P.C. Eklund, *Phys. Rev. B* 59 (1999) 10928.
- [18] C.N.R. Rao, A. Govindaraj, R. Sen, B.C. Satishkumar, *Mater. Res. Innovat.* 2 (1998) 756.
- [19] R.A. Forman, G.J. Piermarini, J.D. Barnet, S. Block, *Science* 176 (1972) 284.
- [20] S. Bandow, S. Asaka, Y. Saito, A.M. Rao, L. Grigorian, E. Richter, P.C. Eklund, *Phys. Rev. Lett.* 80 (1998) 3779.
- [21] J.M. Cowley, P. Nikolaev, A. Thess, R.E. Smalley, *Chem. Phys. Lett.* 265 (1997) 379.
- [22] H.D. Sun, Z.K. Tang, J. Chen, G. Li, *Solid State Commun.* 109 (1999) 365.
- [23] S.A. Chesnokov, V.A. Nalimova, A.G. Rinzler, R.E. Smalley, J.E. Fischer, *Phys. Rev. Lett.* 82 (1999) 343.
- [24] M. Hanfland, H. Beister, K. Syassen, *Phys. Rev. B* 39 (1989) 12598.
- [25] B. Weinstein, R. Zallen, in: M. Cardona, G. Güntherodt (Eds.), *Light Scattering in Solids*, vol. IV, Springer, Berlin, 1984.
- [26] A.K. Sood, Pallavi V. Teredesai, D.V.S. Muthu, R. Sen, A. Govindaraj, C.N.R. Rao, *Phys. Status Solidi (b)* 215 (1999) 393.
- [27] J. Tersoff, R.S. Ruoff, *Phys. Rev. Lett.* 73 (1994) 676.
- [28] A.F. Goncharov, *JETP Lett.* 51 (1990) 418.
- [29] D.W. Snoke, Y.S. Raptis, K. Syassen, *Phys. Rev. B* 45 (1992) 14419.
- [30] S. Ijima, C. Brabec, A. Maiti, J. Bernholc, *J. Chem. Phys.* 104 (1996) 2089.